like (Ba,K)BiO_3 (see ref. 8, for example) is transparent, the electronic equivalency is not as obvious. An electronic analogy is also possible, however, between these seemingly completely different materials. For the oxide perovskites, the electronic states at the Fermi energy involve holes in the oxygen electronic orbitals. The Ni in the $MgCNi_3$ perovskite, which is structurally equivalent to O in the oxides, may also be found to have holes in its electronic orbitals at the Fermi energy. Owing to the nearly filled *d* orbitals in elemental nickel, intermetallic compounds of Ni, especially in the presence of electropositive elements such as Mg, often have filled or nearly completely filled Ni *d* states. If this is the case for $MgCNi_3$, then the conduction will involve holes in Ni *d* states, in an electronic analogy to the holes in the O *p* states in the perovskite oxide superconductors. The fact that superconductivity rather than ferromagnetism occurs in a compound where so much nickel is present is surprising, and suggests that $MgCNi_3$ is a candidate compound for unconventional superconductivity. □

Received 6 March; accepted 5 April 2001.

1. Rice, T. M. Unconventional superconductors: contrasting cuprates and ruthenates. *Physica C* **341–348,** 41–46 (2000).
2. Cava, R. J. *et al.* Superconductivity in the quaternary intermetallic compounds $LnNi_2B_2C$. *Nature* **367,** 252–253 (1994).
3. Scheil, E. & Huetter, L. Zur Kennetis des Systems Nickel-Kohlenstoff-Magnesium. *Z. Metallk.* **44,** 387–389 (1953).
4. Huetter, L. J. & Stadelmaier, H. H. Ternary carbides of transition metals with aluminum and magnesium. *Acta Metall.* **6,** 367–370 (1958).
5. Nohara, M., Isshiki, M., Takagi, H. & Cava, R. J. Magnetic field dependence of the low-temperature specific heat of the borocarbide superconductor, $LuNi_2B_2C$. *J. Phys. Soc. Jpn* **66,** 1888–1891 (1997).
6. Kresin, V. Z. & Parchomenko, V. Thermodynamic properties of strong-coupling superconductors. *Sov. Phys. Solid State* **16,** 2180–2184 (1975).
7. Kresin, V. Z. On the critical temperature for any strength of the electron–phonon coupling. *Phys. Lett. A* **122,** 434–438 (1987).
8. Chamberland, B. L. in *Chemistry of Superconducting Materials* 2–104 (ed. Vanderah, T. A.) Noyes, Park Ridge, NJ, 1992).

Acknowledgements

This research was supported by grants from the US National Science Foundation and the US Department of Energy.

Correspondence and requests for materials should be addressed to R.J.C. (e-mail: rcava@princeton.edu).

Atomic-beam alignment of inorganic materials for liquid-crystal displays

P. Chaudhari*, James Lacey*, James Doyle*, Eileen Galligan*, Shui-Chi Alan Lien*, Alesandro Callegari*, Gareth Hougham*, Norton D. Lang*, Paul S. Andry*, Richard John*, Kei-Hsuing Yang*, Minhua Lu*, Chen Cai*, James Speidell*, Sampath Purushothaman*, John Ritsko*, Mahesh Samant†, Joachim Stöhr†, Yoshiki Nakagawa‡, Yoshimine Katoh‡, Yukito Saitoh‡, Kazumi Sakai‡, Hiroyuki Satoh‡, Shuichi Odahara‡, Hiroki Nakano§, Johji Nakagaki§ & Yasuhiko Shiota§

* *IBM Watson Research Centre, PO Box 218, Yorktown Heights, New York 10598, USA*
† *IBM Almaden Research Centre, 650 Harry Road, San Jose, California 95120-6099, USA*
‡ *IBM Japan Ltd, Display Business Unit, Yamato-shi, Kenagawa-ken, Japan*
§ *IBM Japan Ltd, Advanced Manufacturing Engineering, Yasu-gan, Shiga-ken, Japan*

The technique used to align liquid crystals—rubbing the surface of a substrate on which a liquid crystal is subsequently deposited[1–3]—has been perfected by the multibillion-dollar liquid-crystal display industry. However, it is widely recognized that a non-contact alignment technique would be highly desirable for future generations of large, high-resolution liquid-crystal displays. A number of alternative alignment techniques have been reported[4–7], but none of these have so far been implemented in large-scale manufacturing. Here, we report a non-contact alignment process, which uses low-energy ion beams impinging at a glancing angle on amorphous inorganic films, such as diamond-like carbon. Using this approach, we have produced both laptop and desktop displays in pilot-line manufacturing, and found that displays of higher quality and reliability could be made at a lower cost than the rubbing technique. The mechanism of alignment is explained by adopting a random network model of atomic arrangement in the inorganic films. Order is induced by exposure to an ion beam because unfavourably oriented rings of atoms are selectively destroyed. The planes of the remaining rings are predominantly parallel to the direction of the ion beam.

Here we describe a display manufacturing process that breaks away from the method of the past two decades and compare the process with a model for the atomic-scale mechanism of alignment of liquid crystals. Our understanding of the mechanism enabled us to transfer, within a few years, an experimental process to the manufacturing floor. We first discuss the advantages of the new process over rubbing in display manufacturing, and then we compare some experimental data with the model for alignment.

It is widely believed that the current rubbing manufacturing process has serious limitations. It introduces debris, which means that the rubbing machine must be housed in a separate room, in an otherwise clean-room environment, which is more expensive. It is sometimes unreliable: if the rubbing roller degrades unevenly, the effect of a local defect may not be detected until hundreds of flawed displays have been manufactured and subsequently discarded.

Rubbing can also produce an electrostatic discharge that can adversely influence the electronic circuitry just below the surface of the rubbed polyimide thin film. Rubbing can leave streaks, which degrades the quality of the image. This problem has become more acute as the display resolution has increased and the spacer balls, currently used to separate the two glass plates, are replaced by posts. These posts produce shadows as the roller traverses them, resulting in poor alignment of the liquid crystal in the shadowed area that, because of contrast variations, is visible.

There are two reasons why the rubbing process has been very difficult to displace in liquid-crystal manufacturing: much research and development has been focused on refining the existing process

Figure 1 A photograph of a laptop computer showing a 13.3 diagonal extended graphics array (XGA) thin-film transistor liquid-crystal display using a diamond-like carbon (DLC) film as the alignment layer. An ion beam was used to produce the alignment.

empirically, and any new technology has to satisfy many technical, reliability, cost, and, increasingly, environmental requirements besides improved alignment of liquid crystals. But we believe the process described here meets these challenges.

We have replaced the polyimide (PI) film, which is printed and then baked in a furnace before rubbing, by a cost-effective, one-step evaporated or sputtered film deposited at room temperature. The vapour-deposition process is not only more cost-effective but also more environmentally friendly than the PI, for which relatively large amounts of organic materials and solvents are needed.

We find that a great variety of optically transparent and insulating films, such as hydrogenated diamond-like carbon (DLC), SiN_x, hydrogenated amorphous silicon, SiC, SiO_2, glass, Al_2O_3, CeO_2, SnO_2, $ZnTiO_2$ and $InTiO_2$ can be used as alignment materials. The films are either amorphous or have a very fine grain size. Of these materials we have examined two films in some detail. These are DLC and SiN_x. We have chosen these two materials because of their wide use in electronics, including the display industry. For example, DLC is widely used in disk storage as the final hard layer on disks, and SiN_x is extensively used in the display industry as an insulator. Selecting materials on this basis has the advantage that tools and a knowledge base exist for large-scale manufacturing. Here we use DLC as the prototypical material.

We have replaced the rubbing roller by a low-energy ion gun, available commercially. There is thus no need to wash a rubbed surface to remove debris or to bake it in a furnace to remove the effects of washing. There are also no reliability issues associated with the unpredictable local degradation of the roller. We have manufactured displays, both the twisted nematic displays (15-inch) used in laptops and the in-plane switching displays (22-inch) used in desktops, that show superior front-of-screen quality to displays produced by the rubbing process, primarily because of the absence of rubbing streaks. The new process is more efficient because it is a nonstop manufacturing process; the rubbing technology needs cloth changes, which cause delays in production. An example of a laptop computer display manufactured with the new process is shown in Fig. 1.

Carbon films absorb light in the visible range, whereas polyimide (PI) layers are transparent in the visible. We therefore studied DLC films that are 2–10 nm thick. Figure 2a shows transmittance curves as a function of wavelength of light of a DLC and a PI film. Both films are deposited on glass substrates coated with indium tin oxide. The thickness of the DLC film is about 3–4 nm and that of the PI film is about 60 nm. The PI layer seems to have higher transmittance at short wavelengths around 380 nm whereas the carbon films have higher transmittance in the long wavelength range from about 650 to 800 nm.

We have measured the transmission of white light through cells containing liquid crystals (twisted nematics) and either DLC or PI films. The hydrogen content and thickness of the DLC film were adjusted so that the overall transmission of the cell was at least 95% of the PI-containing cells. We obtained typical values of 97%. Also, from data of the type shown in Fig. 2a, we determined the optical constants of our films, and hence calculated the transmission of light through our cells with Berreman's 4×4 matrix method[8]. We find the agreement between experiment and calculation to be within 1%.

We show, in Fig. 2b, the transmission of light through two twisted nematic test panels as a function of applied voltage across a cell. The cell spacing is about 5 μm. One of the cells contains a DLC film that has been aligned with an ion beam and the other cell contains a polyimide film aligned by rubbing. The transmission characteristics are very similar for the two panels both at zero and finite voltage. The two sets of data were normalized to unity at zero voltage for the purposes of comparison. Visually, the difference in quality of the two panels is indistinguishable. We also measured the charge retention of these two panels. The ion-beam-aligned DLC had a charge retention of 98%; for the rubbed and aligned test panel it was 97.75% that is, essentially the same.

The ion beam produces alignment with pre-tilt angles ranging from values close to zero to about 10°. A pre-tilt, that is, a tilt of the liquid-crystal axial director away from the plane of the surface, is essential in breaking symmetry and producing a uniform display with high contrast. We found that the pre-tilt angle is a function of

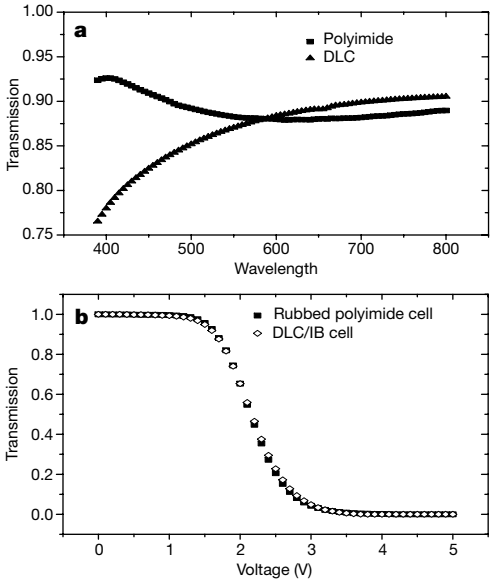

Figure 2 Transmission of light through polyimide and the DLC films on glass substrates and in cells filled with liquid crystals. **a**, Transmission of light through a film of polyimide and DLC deposited on an indium tin oxide coated glass substrates as a function of the wavelength of light. **b**, The transmission of light as a function of applied voltage across twisted nematic liquid-crystal cells made of polyimide and DLC films, as alignment layers.

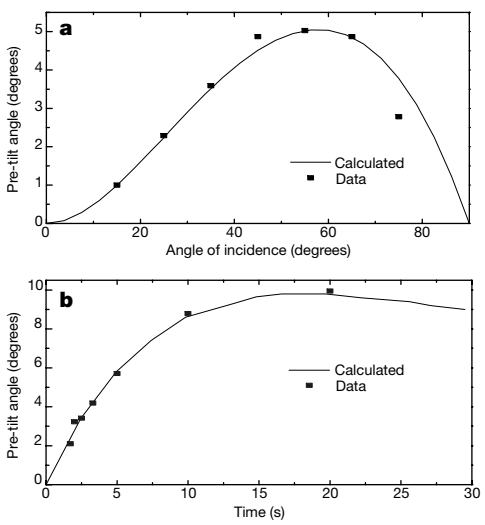

Figure 3 The pre-tilt angle of the liquid crystal as a function of the angle of incidence of the ion beam and time of exposure. All angles are measured from the surface of the substrate. **a**, The pre-tilt angle as a function of the angle of incidence of the ion beam. The film was irradiated with argon ions accelerated to 100 eV, the beam current was 100 mA, and time of exposure was held constant at 30 s. **b**, The pre-tilt angle of the liquid crystal as a function of time of exposure to an argon ion beam. The angle of incidence was held constant at 35 degrees, the acceleration voltage of 200 eV, and the beam current at 100 mA.

the angle of incidence of the ion beam, irradiation times, and ion-beam energy. These findings are similar to our earlier results on the effects of ion beams on polymers[9]. We show in Fig. 3a the pre-tilt angle plotted as a function of the angle of incidence of the ion beam. The data shows a peak in the value of the pre-tilt angle at an incidence angle of the ion beam of about 55°. However, the position of this peak can shift with the time of exposure and the ion beam energy. We show in Fig. 3b the value of the pre-tilt angle as a function of exposure time. This too shows a maximum, whose location changes with the angle of incidence and ion beam energy. It is clear that any desired pre-tilt angle, between approximately 0 and 10° can be obtained by a combination of the angle of incidence of the ion beam and time of exposure.

Another parameter that is important for the functioning of displays is called image sticking. This arises from residual charges that accumulate in a local region as the voltage is left on. When the voltage is removed, the image survives and gradually fades away with time as the charge is dissipated. We have attempted to measure image sticking in a number of twisted nematic cells used in laptops, but so far it has been negligible and less than what we find in rubbed polyimide samples. Image sticking has often been a limiting phenomenon in the acceptance of new ideas to replace the rubbing process.

One interesting phenomenon in rubbing is the ability to overwrite the alignment produced by aligning first in one direction and then rubbing over it in a different direction. This has the advantage of reducing the number of masking steps required in producing a multi-domain display—such a display is characterized by discrete alignment directions of the liquid crystal. We found that the ion beam can also be used to overwrite a previously aligned area. We used this observation to form a two-domain pattern using a single masking step. We first exposed the entire sample to an ion beam and then, using a contact metal mask, selectively exposed the rest of the area in a direction rotated by 180° from the first exposure. We thus fabricated a twisted nematic, two-domain cell in the laboratory. The measured contrast ratio contour, as a function of viewing angle, of such a cell is shown in Fig. 4a. We compared it with the measured contrast ratio contour, as a function of viewing angle, of a single-domain cell shown in Fig. 4b. We note, however, that the contact metal mask is not the best way of producing two domains in a manufacturing environment. A better method would be to use a noncontact metal mask and the properties of ion beams to scan and produce the second domain. We are working on this possibility in the laboratory. However, for desktop displays, where battery lifetime is not an issue, it is possible to use an in-plane switching approach and produce one- or two-domain displays by appropriate design of the switching fields. This is the approach we have taken in producing the high-resolution, two-domain 22-inch display in a manufacturing environment by the process described here. This display currently has the best existing resolution for large displays. It has 3,840 by 2,400 (about 9.2 million) pixels.

We now present a model for the rearrangement of atoms on the surface of an alignment layer produced by a low-energy, collimated ion beam. We assume that the alignment layer is amorphous and isotropic. By isotropic, we mean that the atomic arrangement has no preferred direction before the ion beam is turned on. For the purposes of demonstrating our model, we shall assume that the atomic arrangement can be described by a random network. This is appropriate for covalently bonded solids. However, the precise topology is not important in our modelling. If, for example, the surface is described by a dense random packing of hard spheres, as is generally the case for metallic bonding, we know that there is a transformation that enables us to go from a random network to a dense packing of hard spheres[10]; thus the generality of our argument is still valid.

The topology of a network can be described in terms of ring statistics. For example, a random network describing amorphous silicon contains six-fold, five-fold and seven-fold rings. The orientation of these rings, that is, the vector normal to the plane of the rings, is uniform in all directions. The rings present an anisotropic cross-section to the incoming ion beam. For example, if the ion beam is normal to the plane of the ring it has a much larger probability of interaction than if the ion beam is parallel to the plane of the ring. We use this selectivity, as in Darwin's theory of evolution, to destroy rings that present a larger cross-section than others.

After exposure to an ion beam, what is left behind are predominantly those rings whose ring vector is perpendicular to the ion-beam direction. The liquid-crystal molecules are sensitive to the surface arrangement of atoms and hence align along a direction defined by the ion-beam direction projected onto the surface of a sample. The pre-tilt angle of the liquid crystals is generated, in this model, by those rings whose plane is parallel to the direction of the ion beam.

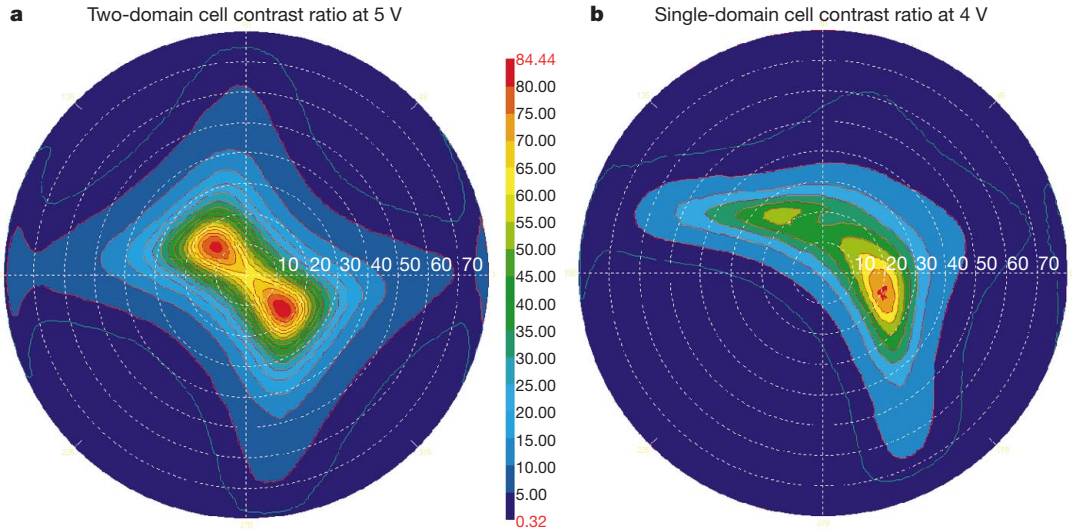

Figure 4 The transmission contrast ratio contours measured as a function of viewing angle for one- and two-domain nematic liquid crystal cells. **a**, Contrast ratio curves obtained from two domains. The second domain was produced using a metal mask with a feature size of about 180 μm. The metal mask was 75 μm thick and made of molybdenum. It was held in contact with the DLC film during ion beam exposure. **b**, Contrast ratio from a single domain.

A comparison of the calculated and measured values of the pre-tilt angles are shown in Fig. 3a and b. The values of the pre-tilt angles were calculated using the equation described in the Methods section. For purposes of comparison with our experiments, we have adjusted the model calculations to match at one point of the pre-tilt versus ion-beam angle and pre-tilt versus ion-beam exposure time data. We note that the model predicts quite well the functional dependence of the pre-tilt angle with angle and time of exposure. A more detailed description of the model and its comparison with experiments, using both liquid-crystal and X-ray data, will be provided elsewhere (P.C., N.D.L., M.S., J.S. and J. Lüning, unpublished work). □

Methods

Optimization of hydrogen content in DLC films

The DLC films were deposited by plasma-enhanced chemical vapour deposition on glass substrates coated with a conducting indium tin oxide (ITO) film about 300 Å thick. Other substrates, such as Si and quartz, were also used for process comparison. The amorphous (a)-C : H films were deposited using C_2H_2/He and H_2 gas mixtures. Hydrogen was added to the process to increase film transmittance. The hydrogen content of the films was measured by forward recoil scattering. We used a process matrix to establish which process parameters yield higher hydrogen content and thus higher transmittance. In all of these experiments, the substrates were held at room temperature, which is important for cost considerations and also helped to obtain more transparent films than would a high-temperature process.

Ion-beam exposure

Ion beams were produced with a direct-current Kaufman-type ion source using a tungsten filament to supply electrons to the plasma and a plasma-bridge neutralizer to maintain charge neutrality. Argon was introduced into the ion source and plasma-bridge neutralizer using separate gas-flow controllers. The plasma-bridge neutralizer has the advantage of reduced substrate contamination as it is not physically immersed in the ion beam. In contrast, the commonly used tungsten-filament neutralizer, which is placed directly in the ion beam, is subject to sputtering by the energetic argon ions and neutrals impinging on it. Ions with energies in the range of 50–500 eV were extracted for the plasma within the ion source and accelerated toward the substrate. Ion current densities were measured using biased Faraday-cup probes to repel low-energy electrons introduced into the beam by the plasma-bridge neutralizer.

Substrates were mounted on a moving stage that was linearly scanned beneath the ion source. The tray speed was programmable, allowing different ion doses to be applied to the sample when using a fixed ion current density. The incident angle of the impinging ions could be varied by adjusting the angular position of the ion source relative to the substrate.

Calculation of the pre-tilt angle as a function of ion beam conditions

We quantify the model, described qualitatively in the text, by assuming that the destruction probability for a ring is proportional to the beam flux through it, and that we can neglect the effect of the destruction of other rings on that of a given ring. Let us assume a coordinate system with **x** normal to the surface and the ion beam incident in the x–y plane towards positive **z**, with angle of incidence α relative to the **z** axis. We define a vector **n** normal to a given ring, and denote the angle between **n** and the **z** axis as θ, and the azimuthal angle in the x–y plane as ϕ.

We denote by $\langle\theta\rangle$ the mean value of θ over the distribution of rings remaining on the surface at a time t, with beam exposure starting at $t = 0$. At $t = 0$, $\langle\theta\rangle = \pi/2$, because the beam distribution starts out isotropic. We take the product, denoted by W, of $\pi/2 - \langle\theta\rangle$ and the fraction of rings remaining on the surface at time t to be a measure of the pre-tilt angle; given the symmetry of the problem, we find that

$$W = \frac{1}{\pi}\int_0^{\pi}\left(\frac{\pi}{2} - \theta\right)\sin\theta\,\mathrm{d}\theta\int_0^{\frac{\pi}{2}}\exp(-pt\sin\alpha|\sin\alpha\sin\theta\cos\phi - \cos\alpha\cos\theta|)\,\mathrm{d}\phi$$

where p is proportional to the beam intensity, ring area, and destruction probability per unit time per unit beam flux through a ring. Using this equation, we have calculated the variation in the pre-tilt angle with the ion-beam dose and its angle of incidence. For details of the model, see P.C., N.D.L., M.S., J.S. and J. Lüning, unpublished work).

Received 30 November 2000; accepted 19 March 2001.

1. DeGennes, P. G. & Prost, J. *The Physics of Liquid Crystals* 161 (Clarendon, Oxford, 1993).
2. Stöhr, J. *et al.* Microscopic origin of liquid crystal alignment on buffed polymer surfaces. *Macromolecules* **31,** 1942–1946 (1998).
3. Stöhr, J. & Samant, M. G. Liquid crystal alignment by rubbed polymer surfaces: A microscopic bond orientation model. *J. Electron Spectrosc. Rel. Phenom.* **98–99,** 189–207 (1999).
4. Aoyama, H., Yamazaki, Y., Matsura, M., Mada, H. & Kobayashi, S. Alignment of liquid crystals on the stretched polymer films. *Mol. Cryst. Liq. Cryst.* **72,** 127–132 (1981).
5. Ikeno, Y. *et al.* Electrooptic bistability of a ferroelectric liquid crystal device using polyimide Langmuir–Blodgett orientation films. *Jpn J. Appl. Phys.* **27,** L475–L476 (1998).
6. Janning, J. L. Thin film surface orientation for liquid crystals. *Appl. Phys. Lett.* **21,** 173–174 (1972).
7. Schadt, M., Seiberle, H. & Schuster, A. Optical patterning of multi-domain liquid-crystal displays with wide viewing angles. *Nature* **381,** 212–215 (1996).
8. Berreman, D. W. Optics in stratified and anisotropic media: 4 × 4-matrix formulation. *J. Opt. Soc. Am.* **62,** 502–510 (1972).
9. Chaudhari, P., Lacey, J., Lien, S. A. & Speidell, J. L. Atomic beam alignment of liquid crystals. *Jpn J. Appl. Phys.* **37,** L55–L56 (1998).
10. Chaudhari, P., Graczyk, J. F., Henderson, D. & Steinhardt, P. Transformation between random network and dense random-packed models for amorphous solids. *Phil. Mag.* **31,** 727–732 (1975).

Acknowledgements

We thank T. Hashimoto for his encouragement and T. Ueki, H. Yamaguchi and M. Mitsuhashi for their sustained suport. P.C. thanks N. Okazaki for describing this technology to colleagues in Japan. G. Thompson photographed Figure 1.

Correspondence and requests for materials should be addressed to P.C. (e-mail: chaudha@us.ibm.com).

Size-dependent control of the binding of biotinylated proteins to streptavidin using a polymer shield

Zhongli Ding, Robin B. Fong, Cynthia J. Long, Patrick S. Stayton & Allan S. Hoffman

Department of Bioengineering, University of Washington, Seattle, Washington 98195, USA

Many medical and biotechnological processes rely on controlling and manipulating the molecular-recognition capabilities of proteins[1–4]. This can be achieved using small molecules capable of competing for protein binding or by changing environmental parameters that affect protein structure and hence binding. An alternative is provided by stimuli-responsive polymers that change reversibly from a water-soluble expanded coil to a water-insoluble collapsed globule upon small changes in temperature, pH or light intensity: when attached to proteins in the vicinity of their binding sites, they reversibly block and release small ligands[1,5–7]. Here we show how this approach can be extended to achieve size-selective binding of large, macromolecular ligands. We use the thermally responsive polymer poly(*N*,*N*-diethylacrylamide) (PDEAAm), and attach it to the protein streptavidin approximately 20 Å from the binding site for biotinylated proteins. Below the lower critical solution temperature of PDEAAm, the polymer is in its extended state and acts as a 'shield' to block the binding of large biotinylated proteins; above this temperature, it collapses and exposes the binding site, thereby allowing binding. We find that the degree of shielding depends on both the size of the biotinylated protein and the size of PDEAAm, suggesting that 'smart' polymer shields could be tailored to achieve a wide range of size-dependent ligand discrimination for use in affinity separations, biosensors and diagnostics technologies.

We have previously described the conjugation of stimuli-responsive polymers to genetically engineered sites near the binding site (or pocket) of streptavidin, yielding 'affinity switches' that control the binding and release of the small ligand biotin through small changes in environmental conditions[1,5–7]. The stimuli-responsive polymers reversibly cycle between an expanded coil and a collapsed globule in response to small changes in temperature, pH, or light, with a change in hydrodynamic radius of about three times[8]. In our previous work, the polymer was attached very close to one of